

Enhancing Aircraft Ground Trajectories through Map-Matching and Stochastic Pavement Roughness Modeling

Martin Schlosser,* Hannes Braßel, and Hartmut Fricke 

TUD Dresden University of Technology, Chair of Air Transport Technology and Logistics, Dresden, Germany

*Corresponding author: martin.schlosser@tu-dresden.de

(Received: 1 November 2024; Revised: 13 February 2025; Accepted: 13 February 2025; Published: 22 February 2025)

(Editor: Xavier Olive; Reviewers: Manuel Waltert and Rainer Koelle)

Abstract

Predictive maintenance is essential in aviation due to rising cost pressures, leveraging sensor data and maintenance logs for improving planning efficiency. Analyzing historical data ensures timely interventions, reducing unplanned downtime and enhancing aircraft reliability. Digital twin applications expand these capabilities, allowing precise monitoring and proactive analyses of aircraft components, tracking stress, fatigue, and health conditions. Accurate load monitoring during ground operations requires integrating actual aircraft trajectories with environmental factors like pavement conditions and weather, which can pose challenges due to data sparsity, noise, or misalignment. Our study outlines a methodology using sparse Automatic Dependent Surveillance-Broadcast (ADS-B) and geospatial airport data, employing map-matching and filtering techniques for comprehensive trajectory representation and analysis. Additionally, we introduce roughness-specific pavement stochastic modeling to allow load assessment on aircraft structures during ground roll including surface irregularities and damage patterns. This model precedes a probabilistic fatigue model, aiming to initially diagnose potential structural issues to enable subsequent prediction, and mitigate efforts, thereby enhancing aircraft durability and thus operational safety.

Keywords: Trajectory Modeling; Map-matching; Surface Modeling; Aircraft Ground Maneuvers; Aircraft Component Safety

Abbreviations: ADS-B: Automatic Dependent Surveillance - Broadcast, AOA: Airport Operational Areas, OSM: OpenStreetMap, PSD: Power Spectral Density, RWY: Runway, TWY: Taxiway.

1. Introduction

The surge in air traffic volume and the intricate operations at airports present challenges for ensuring the safety and efficiency of aircraft ground movements. The traffic density on runways (RWY), taxiways (TWY), and aprons complicates taxi routing, especially in airports with complex layouts and procedures. These complexities lead to extended taxiing distances, frequent braking, acceleration, and turning maneuvers. As a result, aircraft tires and landing gears are exposed to significant dynamic loads, affecting their health status and thereby impacting components' safety. However, conventional maintenance routines often rely on fixed schedules, with data constraints limiting predictive measures and the adoption of demand-driven assessments. In this context, digital twin technology emerges as a promising tool for monitoring component health in a digital environment, assessing stress and fatigue spectra during ongoing operation, enhancing component life cycle management, optimizing certification processes from the manufacturer's perspective, and enabling pre-

dictive maintenance [1, 2, 3, 4]. For this purpose, comprehensive simulation approaches gathering and processing data are required to accurately model landing gear behavior and condition in a virtual environment, e.g., regarding structural loads during operations, corrosion effects, and maintenance history. For developing a load monitor for aircraft landing gears during ground operations as part of a safety-driven digital twin framework, tire and landing gear properties and behavior, aerodrome pavement roughness, RWY condition, and aircraft maneuvers derived from trajectory data must be considered. Notably, the use of open-access trajectory data derived from *OpenSky Network* [5] is a key strength of the methodology presented in this study, as it allows stakeholders without access to proprietary aircraft-logged data, such as Flight Data Monitoring (FDM) information, to replicate and implement our approach effectively.

The essential modeling requirements for this purpose (cf. Figure 1) encompass a bottom-up approach, covering:

- **Modeling of ground trajectories** from *Automatic Dependent Surveillance-Broadcast* (ADS-B) data by deriving trajectories from aircraft position and determining movement parameters, for example speeds, acceleration, steering angles,
- **Stochastic modeling of RWY/TWY roughness** accounting for surface variations induced by design-related irregularities (e.g., concrete joints, or inset lights) or typical damage patterns (e.g., cracks, pop-outs),
- **Tire-pavement interaction modeling** utilizing a calibrated tire model, and
- **Aircraft tricycle rigid body motion model** with six degrees of freedom, integrating tire and oleo strut models to calculate forces and moments at the landing gear incorporating the aforementioned modeling aspects.

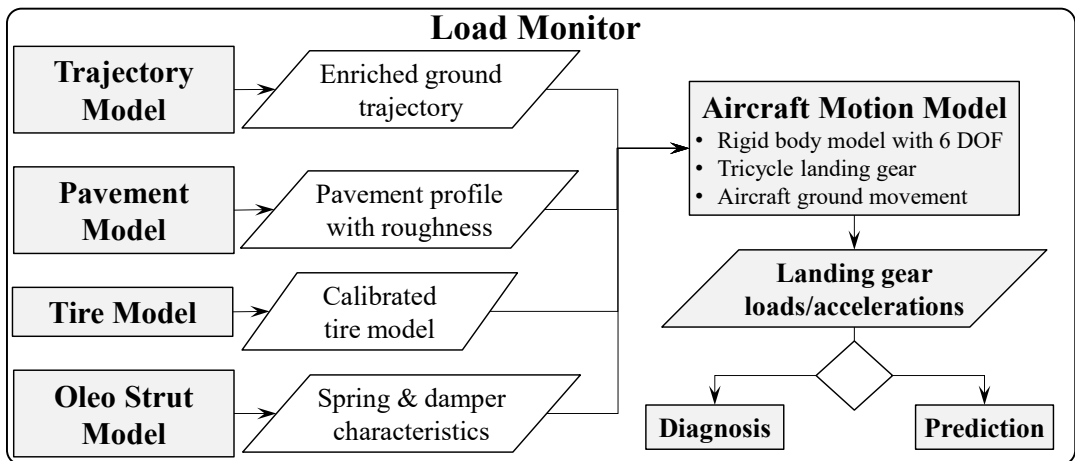


Figure 1. Flowchart of the relevant models within the load monitor.

This modeling approach incorporates key motion parameters like ground speed and steering angle for post-operative trajectory replication, requiring consistent and realistic trajectory data with adequate parameter coverage, accuracy, and resolution. However, aircraft position data often suffer from sparse, noisy, or temporally and spatially misaligned data points due to sensor-based measurements and coverage issues, which can be particularly significant for certain airports, especially for ground trajectories recorded in the *OpenSky Network* [5] (cf. Figure 2). These coverage limitations result in only a few airports where *OpenSky Network* [5] provides high-quality ground trajectory data (e.g., Zurich Airport). To address these challenges, our focus is on developing a robust methodol-

ogy for processing and analyzing aircraft ground trajectories, employing map-matching techniques with open-source data to enrich sparse input trajectories and partially overcome the limitations of OpenSky Network [5] ground data.

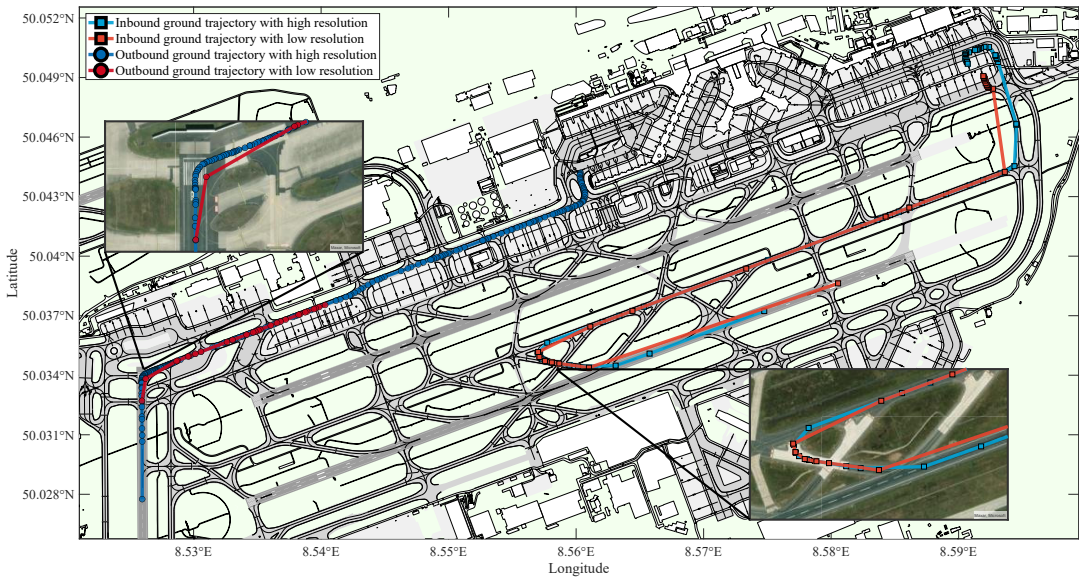


Figure 2. Comparison of exemplary samples from ADS-B OpenSky Network [5] dataset at Frankfurt Airport (EDDF) for inbound (landings on RWY 25L) and outbound (takeoffs from RWY 18) with different data quality: ground trajectories with higher temporal resolution (blue) and ground trajectories with lower one (red).

Additionally, we also developed a model that allows for the stochastic generation of pavement surface macrotexture in order to add roughness criteria to the analyzed trajectories based on [6]. The pavement roughness or unevenness significantly influences the tire-pavement interaction that substantially affects the dynamic loads and vibrations acting on the landing gear during ground operations incorporating takeoff and landing run as well as taxiing [7]. The influence of pavement roughness on aircraft structure in terms of fatigue and dynamic stresses, performance, its occupants (esp. passenger/pilot comfort) and thus operational safety (e.g., [8, 9, 10, 11]) has been subject to the scientific discourse for several years and remains an ongoing topic (e.g., [12, 13]). Irregularities in the pavement's surface arise from normal tolerances of engineering standards required for construction, such as concrete joints, or aerodrome design-related requirements including inset lights or markings. Additionally, wear and tear caused by chemical influences, especially use of de-icing agents, meteorological factors like temperature fluctuations, and mechanical forces for example surface loading by aircraft undercarriages and other aerodrome vehicles can lead to surface material fatigue, resulting in typical damage patterns such as cracks and thus unevenness [7, 14]. Thus, we employ methods for generating artificial fractal surfaces by applying power spectral density (PSD) according to [15]. These surfaces incorporate both design-related variations and specific damage patterns, resulting in highly detailed pavement surface with a finely resolved vertical axis. By integrating these modeling techniques, we develop a comprehensive 3D trajectory description, essential for input into our aircraft motion model. This approach enables effective load monitoring as part of a safety-focused digital twin application enabling high fidelity monitoring on component level in a digital environment, enabling the diagnosis of stress and fatigue spectra during ongoing operations, and prediction of future component conditions enhancing insights into component safety.

1.1 State-of-the-Art

1.1.1 Trajectory Modeling and Analysis

Various data sources exist for analyzing aircraft ground trajectories. Onboard systems within the framework of Flight Data Monitoring (FDM) collect extensive data, complying with IR-OPS standards of *European Union Aviation Safety Agency* (EASA) [16], noted for their breadth in parameters and precision. However, access to such data is generally limited (e.g., [17]) and represents a common restriction across studies in the aviation domain, including this one. Similarly, Advanced-Surface Movement Guidance and Control System (A-SMGCS) offer prospects for modeling trajectories [18]; however, these are proprietary to airport operators and rarely public. *Airport Surface Detection Equipment, Model X* (ASDE-X) Data, available through the *NASA Sherlock Data Warehouse*, amalgamates ground traffic data from radar, multilateration (MLAT), and ADS-B for selected U.S. airports [19], providing high-quality datasets, however not covering European airports. Thus, ADS-B, accessible via OpenSky Network [5] and *Flightradar24* (www.flightradar24.com), is widely used (e.g., [20, 21]), yet ground data quality may be compromised by the placement and number of receivers and the status of aircraft transponders.

Numerous scientific publications focus on analyzing sparse trajectory data to extract relevant operational insights and metrics. Hoole *et al.* explore methods to characterize maneuver variability, assessing landing gear load and operational safety [21]. Basora *et al.* address anomalies in trajectory data using statistical analyses like regression and neural network-based reconstruction methods [22], while Olive *et al.* apply machine learning algorithms for outlier detection in Mode S data [23]. Furthermore, anomaly detection and trajectory prediction clustering are examined in [24, 25, 26]

Sparse or inaccurate trajectory processing include inverse sampling (interpolation) and error reduction (smoothing) techniques. These methods cover outlier testing [27], spline-based smoothing [28], and model-based reconstruction using filters like the Kalman filter [29, 24, 30]. Advances in filtering include hybrid statistical models that combine continuous motion estimators and discrete model switching, exemplified by the Interacting Multiple Model Filter (IMM) and Multi-Hypothesis Tracker (MHT) [31, 32]. The influence and effectiveness of various filtering techniques on flight trajectories are analyzed in [33]. Finally, map-matching algorithms, previously applied in road traffic, are increasingly used for analyzing aircraft ground movements, aligning position data with digital map information [18, 34, 35, 36]. A detailed review of these algorithms is presented in [37, 38].

1.1.2 Roughness Description and Modeling

Pavement roughness significantly impacts aircraft performance, component lifespan, and the safety of ground operations. It necessitates adherence to regulatory standards for determining ground loads during aircraft certification [7] and for the design and maintenance of *Airport Operational Areas* (AOA) pavements across Europe [39]. Airport operators conduct regular inspections and maintenance action on AOA pavements, providing detailed pavement condition information [40]. Various methods and devices, from visual inspections to advanced technologies, e.g., LiDAR and photogrammetry via unmanned aerial vehicles (UAV), assess both functional (e.g., material properties) and structural (surface properties, e.g., roughness) conditions of airport pavements [41, 42, 43, 44, 45]. Empirical records of RWY and TWY surface profiles from various international airports primarily inform data on pavement surface profiles. Deterministic dynamic analyses, utilizing actual RWY profiles such as the pre-resurfacing San Francisco RWY 28R [8] as a worst-case scenario, contribute to aircraft certification efforts by assisting in the assessment of landing gear loads during ground operations [7]. The *Federal Aviation Administration* (FAA) repository [41] offers the pavement software *ProFAA* for calculating roughness indices, for instance Boeing Bump Index (BBI), International Roughness Index (IRI) and Pavement Condition Index (PCI) [46, 47, 48], and contains real profiles from RWY and TWY used in FAA studies [49, 50].

In addition, scientific studies explore the effects of roughness on aircraft dynamic responses and

model surface profiles. Methods enhance roughness indices Boeing Bump Index and International Roughness Index [51], introduce landing gear cumulative stroke as an alternative [9], and analyze RWY dynamic responses to aircraft taxiing loads [13]. Investigations assess pavement roughness and taxi speed effects on vertical accelerations in aircraft cockpits and at the center of gravity [12].

Power spectral density (PSD) characterizes surface roughness and its effects on friction and adhesion [52, 15, 53, 54]. Computer simulations are used to investigate adhesive interactions on rough surfaces [55], and fractal-based roughness characterization methods are introduced [56]. PSD analysis predicts functional properties of adhesion and friction [57], while strategies for reconstructing accurate PSDs and their implications on surface topography tuning are discussed [58]. Moreover, methods for estimating airport pavement spectral density [59], characterizing RWY roughness via PSD and spectrum parameters, correlating them with aircraft vibrations [60], and analyzing taxiing-induced vibrations in large aircraft [61] underscore the importance of applying PSD methods in studying random vibrations with consideration for undercarriage dynamics' nonlinearities.

1.2 Scope and Objectives

The objective of this paper as first step towards developing a load monitor (cf. Figure 1) in digital twin applications is to present a methodology for both processing and analyzing aircraft ground trajectories on the movement area from sparse position data as input and stochastic modeling pavement roughness along this trajectory (cf. Figure 4). To address the challenge of data sparsity and enhance ground trajectory analysis, Section 2 introduces our methodology consisting of trajectory enrichment and smoothing with open source data using map-matching methods (cf. Section 2.1). At a sampling rate of 1 Hz [62], the interval between consecutive ADS-B data points can exceed 15 m, driven by taxiing speeds ranging from 8 m s^{-1} to 15 m s^{-1} . This challenge is further exacerbated by potential measurement errors and data loss, particularly evident in curved segments (see Figure 2 and Figure 3). These gaps result in an underestimation of the taxiing distances, which in turn leads to inaccuracies in the calculation of speeds. Given the high forces exerted on the landing gear and aircraft structure during turns, precise distance measurement is essential for ensuring accurate modeling.

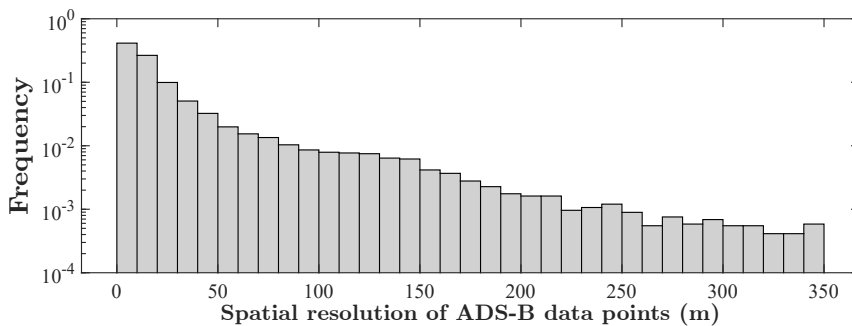


Figure 3. The histogram shows the distribution of spatial resolution for ADS-B data points, representing the distance between consecutive measurements in our dataset. The variability in distances between data points arises from fluctuations in aircraft ground speeds and data irregularities.

Our data-driven approach aims for reconstructing sparse position data points and additionally assigning further infrastructure information to the trajectory and incorporates further analysis of the enriched trajectory, for instance segmentation into turn and straight segments for determining aircraft maneuvering parameters [63]. In Section 2.2, we detail our pavement roughness modeling approach, acknowledging the inherent heterogeneity of pavement surfaces in airport maneuvering areas. As we require a fast and universally applicable modeling approach, and access to precise cur-

rent profile data, e.g., from 3D surface scans, is severely limited (cf. Section 1.1.2), our method opts for stochastically generated scenario data to encompass diverse surface conditions. While existing literature offers detailed pavement modeling techniques using PSD, our approach prioritizes practicality, focusing on enriching ground trajectories with comprehensive roughness information for reliable ground load diagnostics within the digital twin application framework. Our approach does not only aim at determining limit loads but rather emphasizes depicting a full spectrum of ground maneuvering loads during daily operations. This rationale justifies our use of randomized surface generation and integration of design-related irregularities and typical damage patterns. Section 3 applies the previously developed methodology to an exemplary dataset. The results obtained are discussed in Section 4, along with their further application contributing to the development of a load monitor within a digital twin application.

The present paper extends the trajectory generation approach detailed in [63] by applying the methodology to a different OpenSky Network [5] dataset. Furthermore, heading calculations according to Equation (11) were modified and the underlying graph model has been refined for improving the map-matching approach (cf. Section 2.1). The primary distinction, however, is that the generated trajectories are now enriched with surface roughness information, which is critical for load estimation, thereby enabling the derivation of complete 4D trajectories (cf. Section 2.2).

2. Methodology

Our methodology, summarized in Figure 4, comprises two main steps. In Step 1, we enhance ground trajectories derived from sparse ADS-B data using map-matching techniques, complemented by subsequent filtering and smoothing processes to develop a detailed trajectory profile (cf. Section 2.1). Step 1 further involves analyzing these refined trajectories by determining aircraft maneuver parameters, (e.g., ground distance and speed), and employing a segmentation algorithm to classify the trajectory into turns and straight paths (cf. Section 2.2). This segmentation aids in further refining the trajectories and enables detailed analyses of parameters crucial for future trajectory predictions. The third step introduces a stochastic model for the surface on which these trajectories are projected, improving the precision of our predictive models (cf. Section 2.2).

2.1 Ground Trajectory Enrichment, Smoothing and Analysis

For enriching sparse trajectory data, we define the dataset of all tracked aircraft positions as $T = \{(x_i, y_i, t_i)\}_{i=1}^N$, where N represents the total number of position data points across all flights within the dataset, with x_i, y_i as Easting and Northing in *Universal Transverse Mercator* (UTM) format, and t_i as the timestamp for each position. UTM is employed as it provides a consistent, planar coordinate system with minimal distortion at local scales. Its metric framework enables precise and straightforward calculations of distances and speeds, making it particularly suitable for aerodrome surface analysis. Furthermore, *OpenStreetMap* (OSM) [64] is used to provide detailed geospatial data between consecutive aircraft positions, including a node-edge model of airport RWYs, TWYs, and parking positions derived from centerline markings. OSM also offers type, designators, dimensions, and surface material of these features. Another source for acquiring aeronautical information is the *Aeronautical Information Exchange Model* (AIXM), jointly provided by the *European Organisation for the Safety of Air Navigation* (EUROCONTROL) and the FAA (<https://aixm.aero/>). AIXM is an open-source XML file format (current version: AIXM 5.1/5.1.1) and facilitates the transition from traditional paper-based Aeronautical Information Services (AIS), for example the *Aerodrome Information Publication* (AIP), to digital data provision. AIXM offers detailed digital aeronautical information, including aerodromes, airspace structures, routes, and flight restrictions. The provided aerodrome data offers high precision regarding surface markings and lighting and reflects the current state of airports as accurately as possible. The global availability of data for international airports is limited. A list of available datasets for

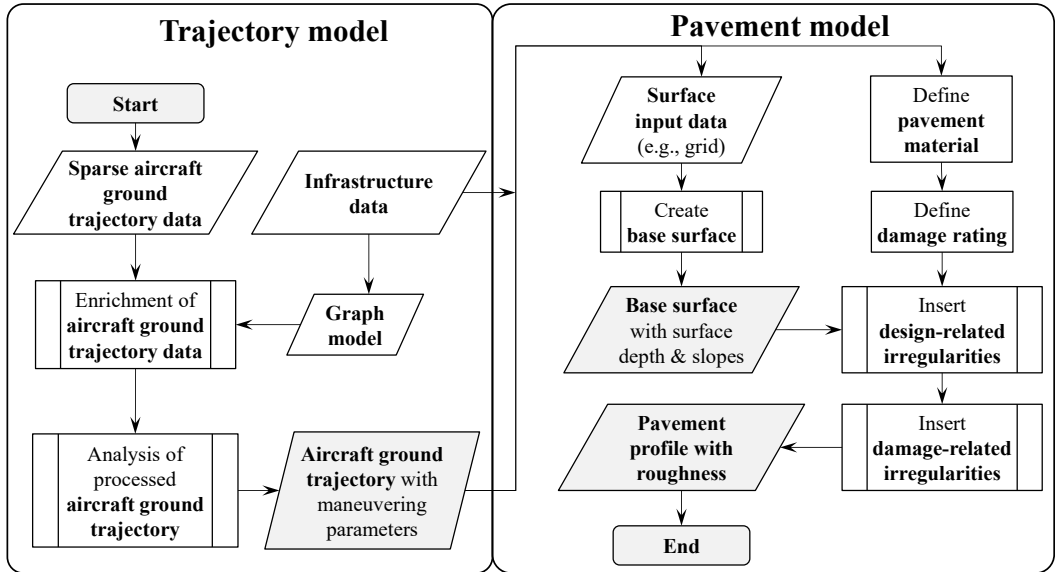


Figure 4. Flowchart showing generalized processing steps within our methodology for trajectory and pavement modeling.

each country can be accessed at https://ext.eurocontrol.int/airm_confluence/display/AIX/Inventory. For this study, the dataset was used as an additional source, providing georeferenced information on RWYs, TWYs, apron areas, and buildings including details such as designators, markings, lighting elements, and pavement materials.

However, transforming the georeferenced information provided by OSM into a graph model for accurate aircraft ground movement enrichment is challenging due to lack of inherent relational data detailing connectivity and transitions between features. To address this, our method linearly interpolates between segment endpoints to identify valid graph edges based on proximity relationships of an equidistant point grid. Each line segment from OSM, S_j , is represented by start $Q_{j,start} = (x_{j,start}, y_{j,start})$ and end points $Q_{j,end} = (x_{j,end}, y_{j,end})$ in UTM coordinates. The length L_j of each segment, measured as the Euclidean distance, is defined by Equation (1):

$$L_j = \|Q_{j,start} - Q_{j,end}\| \quad (1)$$

The spatial resolution criterion, referred to as the proximity threshold ϵ , defines the number of interpolations p for each segment j :

$$p_j = \left\lceil \frac{L_j}{\epsilon} \right\rceil \quad (2)$$

Thereby, $\lceil \cdot \rceil$ represents the ceiling function, which ensures that p_j is an integer and guarantees a minimum spatial resolution for edge identification. The resulting interpolation points are determined as follows, maintaining a consistent spatial resolution:

$$Q_{j,k} = Q_{j,start} + \frac{k}{p_j + 1} \cdot (Q_{j,end} - Q_{j,start}) \quad (3)$$

$$\forall k = \{1, 2, \dots, n\}$$

Figure 5 illustrates the extended OSM data using airport EDDF as an example.



Figure 5. Original centerline data from OSM (circle) and extended/interpolated coordinates (dot) differentiated into AOA at EDDF including their designators.

Then, let us define a set $V = \bigcup_j Q_{j,k}$ by combining vertices from each segment. A distance threshold d_{th} then facilitates the introduction of a function $E : V \times V \rightarrow \{0, 1\}$ to determine if an edge E connecting any two vertices within V is valid:

$$E_{m,n} = \begin{cases} 1, & \text{for } d_{m,n} \leq d_{th} \\ 0, & \text{in other cases} \end{cases} \quad \text{for all } m, n \in V, m \neq n \quad (4)$$

Here, $E_{m,n} = 1$ indicates a valid edge between vertices m and n . To ensure the graph model accurately represents feasible TWY intersections, d_{th} is set slightly above ϵ , compensating for any data inaccuracies. Then, a graph $G(V, E)$ with undirected edges, where self-loops are excluded to avoid redundant connections, serves to predict the path between two consecutive ADS-B data points i and $i + 1$. Compared to [63], the graph model was enhanced by removing unnecessary edges, and by adapting both the distance threshold d_{th} and search radius r_s for identifying valid connections within the map-matching approach. This adjustment enables more precise results, particularly in airport areas characterized by a high density or overlapping of different types of markings within the AOA (cf. Figure 11). The path prediction is realized by executing the following two steps:

1. Map the positions of each flight f , defined as $T_f = \{(x_{f,i}, y_{f,i}, t_{f,i})\}_{i=1}^{N_f}$, to the nearest neighbor graph vertex V .
2. Determine the most feasible route connecting these vertices in the graph model.

Let's introduce a mapping function Φ , which assigns each aircraft position $T_{f,i} = (x_{f,i}, y_{f,i})$ of flight f to the most plausible nearby vertex $k \in V$. The function is defined as follows:

$$\Phi(T_{f,i}) = \operatorname{argmin}_{k \in V} \left(\sqrt{(x_{f,i} - x_k)^2 + (y_{f,i} - y_k)^2} + \gamma_{i,k} M \right) \quad (5)$$

where M is a significantly large number used to penalize incorrect assignments, introduced by the "Big M" method. A plausibility check γ evaluates the orientation alignment of the aircraft's heading

i with the angular orientations of the OSM edges k in the undirected graph G . The check calculates the heading difference $\Delta\theta_{i,k}$ and compares it to an angular threshold α_{th} , ensuring alignment within a predefined tolerance, considering both standard ($|\Delta\theta_{i,k}|$) and perpendicular ($|\Delta\theta_{i,k} + \frac{\pi}{2}|$) alignments:

$$\gamma_{i,k} = \begin{cases} 1 & \text{if } \min(|\Delta\theta_{i,k}|, |\Delta\theta_{i,k} + \frac{\pi}{2}|) \leq \alpha_{th} \\ 0 & \text{otherwise} \end{cases} \quad (6)$$

Then we formulate an optimization problem that seeks to minimize the path's cost to determine the shortest path between two mapped vertices $\Phi(T_{f,i})$ and $\Phi(T_{f,i+1})$:

$$\min_{P_{f,i,i+1} \subseteq G(V,E)} C(P_{f,i,i+1}) = \sum_{(m,n) \in P_{f,i,i+1}} w_{m,n} \quad (7)$$

$$\text{where } w_{m,n} = (1 - E_{m,n}) \cdot M + d_{m,n}$$

subject to:

$$P_{f,i,i+1} \text{ starts at } \Phi(T_{f,i}) \text{ and ends at } \Phi(T_{f,i+1}),$$

$$\forall m, n \in V, m \neq n$$

In this model, $C(P_{f,i,i+1})$ denotes the total cost of the path $P_{f,i,i+1}$, including vertex distances $d_{m,n}$. Using a large penalty factor M for non-viable edges, shortest path algorithms like Dijkstra [65] or A* [66] efficiently find the most cost-effective route. The outcome identifies the optimal sequence of vertices connecting the two mapped points. Then, the original trajectory T_f is augmented by incorporating $T_{f,i}$, intermediate vertices from $P_{f,i,i+1}$ excluding the start and end vertices, and $T_{f,i+1}$ to enrich the ADS-B trajectory with additional positions from the OSM data. For this enriched trajectory of flight f , at data point i and interpolated position α , we introduce the following notation:

$$T_{f,i,\alpha} = (x_{f,i,\alpha}, y_{f,i,\alpha}) \quad (8)$$

Finally, to refine the flight trajectory $T_{f,i,\alpha}$, the Savitzky-Golay filter [67] is employed. This filter smooths data by fitting local polynomials within a moving window, effectively reducing noise while preserving key features regarding peaks and troughs. Applied separately to the x and y coordinates of the enriched trajectory, the operation is described mathematically:

$$x'_{f,i,\alpha} = \sum_{j=-\frac{w-1}{2}}^{\frac{w-1}{2}} c_j \cdot x_{f,i,\alpha+j} \quad (9)$$

$$y'_{f,i,\alpha} = \sum_{j=-\frac{w-1}{2}}^{\frac{w-1}{2}} c_j \cdot y_{f,i,\alpha+j} \quad (10)$$

Here, c_j are the filter coefficients based on the polynomial order, and w is the selected window size. This smoothing process incorporates data from adjacent points to calculate each smoothed coordinate, improving trajectory accuracy by mitigating noise, measurement uncertainties, and map-matching-induced inaccuracies. Figure 6 illustrates the effects of the applied filter using a representative ground trajectory. Particularly in curve segments, the noise is significantly reduced, resulting

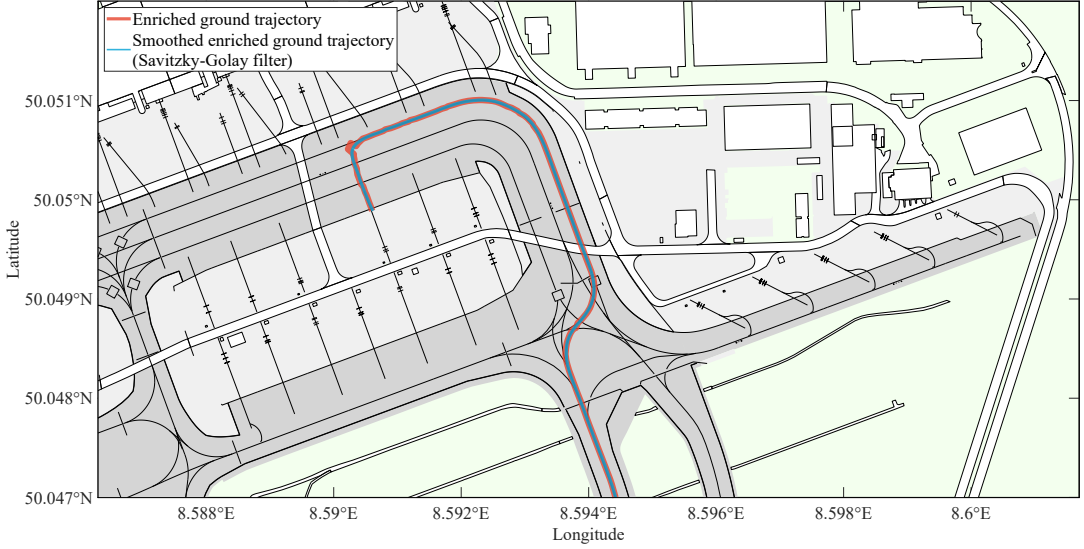


Figure 6. Effect of the Savitzky-Golay filter on the enhanced ground trajectory: comparison of a trajectory section with (blue) and without (red) filtering. The filtered data exhibits more realistic aircraft maneuvering, particularly in curve segments. The text boxes display the designators for the TWYs and aircraft stands.

in a more realistic, smoother trajectory. The output is an augmented taxiing trajectory suitable for analytical analyses, preserving essential features of the original ground path. This enhancement allows for precise computation of taxiing distances, average speeds between aircraft positions, and aircraft headings at each discrete location, with the first two parameters being calculated similarly to Equation (1) and its time derivative. These detailed metrics set the stage for refining our understanding of aircraft heading $\theta_{f,i,\alpha}$ during taxiing by utilizing the Haversine formula:

$$\theta_{f,i,\alpha} = \text{atan2}\left(\cos(x'_{f,i,\alpha+1}) \cdot \sin(y'_{f,i,\alpha+1} - y'_{f,i,\alpha}), \cos(x'_{f,i,\alpha}) \cdot \sin(x'_{f,i,\alpha+1} - x'_{f,i,\alpha}) \cdot \cos(x'_{f,i,\alpha+1}) \cdot \cos(y'_{f,i,\alpha+1} - y'_{f,i,\alpha})\right) \quad (11)$$

The Haversine method provides a more robust and precise calculation compared to that described in [63]. This is particularly evident in the aircraft headings along the RWY centerline, which precisely align with the true RWY bearing as stated in the *Aerodrome Information Publication (AIP)*.

Trajectory segmentation into straight and curved paths uses the change in heading of subsequent discrete positions, which is defined as:

$$\Delta\theta_{f,i,\alpha} = \theta_{f,i,\alpha+1} - \theta_{f,i,\alpha}. \quad (12)$$

By normalizing the heading change to lie between -180° and 180° , we categorize segments as follows:

- Segments where $|\Delta\theta_{f,\alpha}| \leq \Delta\theta_{\text{TH}}$ are classified as straight.
- Segments where $\Delta\theta_{f,\alpha} > \Delta\theta_{\text{TH}}$ are classified as right curves.
- Segments where $\Delta\theta_{f,\alpha} < -\Delta\theta_{\text{TH}}$ are classified as left curves.

Thereby, the threshold $\Delta\theta_{TH}$ compensates for inaccuracies after map-matching smoothing. Note, that $\Delta\theta_{TH}$ is sensitive to the proximity threshold ϵ defined in Equation (2). In our previous work [63], we demonstrated that the map-matching method significantly improves the mapping of ground roll trajectories compared to raw ADS-B data—particularly in depicting taxiing in curved areas and cases of one or more consecutive missing measurements due to disturbances. Following, the enriched trajectory will be expanded using a stochastic pavement roughness model.

2.2 Pavement Roughness Modeling

The starting point for creating stochastic roughness profiles (cf. Figure 4) is the creation of a grid defined by length X , width Y , for example according to the aircraft's wheel track, and the degree of resolution of the pavement to be modeled (cf. Figure 7). The resolution significantly determines the number of resulting nodes. For instance, 1×10^6 nodes result from a pavement surface area of $A = 1 \text{ m}^2$ with a grid resolution of $1 \times 10^{-3} \text{ m}$.

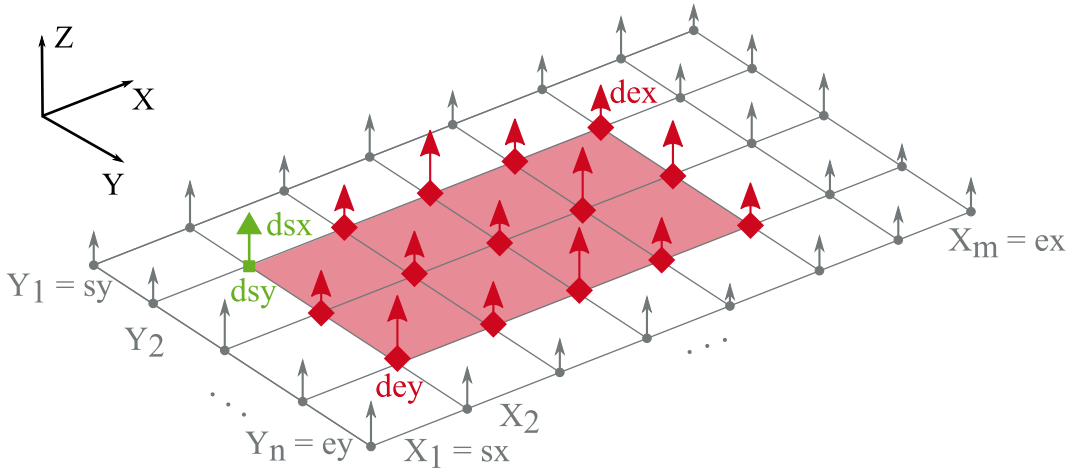


Figure 7. Grid with nodes for the base surface (grey), damage pattern (red), including the damage pattern's start point (green), and indices for the start (s) and end (e) grid points in the X-direction and Y-direction. The nodes for the base surface are denoted as s_x and s_y (start) and e_x and e_y (end), while the start and end nodes for the damage pattern are denoted as ds_x and ds_y (start) and dex and dey (end).

The grid's resolution affects both the level of degree of irregularities resp. damage patterns to be implemented, as well as computational time. The defined grid serves as input for generating the base surface. Both design-related irregularities and typical damage patterns are then inserted, distinguishing between pavement material and damage rating. The base surface is generated using artificial fractal-structured surfaces through PSD. The PSD provides the squared absolute of the Fourier spectrum of the surface profile, encompassing essential details regarding both vertical and lateral profile characteristics. According to [55], randomly rough surfaces can be generated with a typical elevation spectrum $C(q)$ given by

$$C(q) = \left\langle \left| \tilde{h}(q) \right|^2 \right\rangle = \frac{C(0) \Theta(q_s - q)}{\{1 + (q/q_r)^2\}^{(1+H)}} \quad (13)$$

with $\tilde{h}(q)$ as Fourier transform of elevation $h(r)$, $\lambda_r = 2\pi/q_r$ resp. $\lambda_s = 2\pi/q_s$ are the roll-off wavelength (index r) resp. short-wavelength cutoff (index s) and H the Hurst exponent for defining

roughness in the range of $0 \leq H \leq 1$, where larger H values produce smoother surfaces. Detailed information on Equation (13) can be found in [56, 57, 58].

To enhance the practical applicability of PSD within our pavement modeling approach, we utilized a surface generator providing artificially random rough surfaces available from the *MATLAB* repository. Function *artificial_surf* [68] based on prior works by Kanafi *et al.* [15, 54, 53] was applied to the defined grid and adapted enabling the implementation of longitudinal and cambered transverse slopes of RWY/TWY. Figure 8 shows an exemplary base surface with dimensions of $0.1 \text{ m} \times 0.1 \text{ m}$. It is important to note that the elevation values (z-axis and color bar) are given in $10^{-3} \text{ m} = 1 \text{ mm}$.

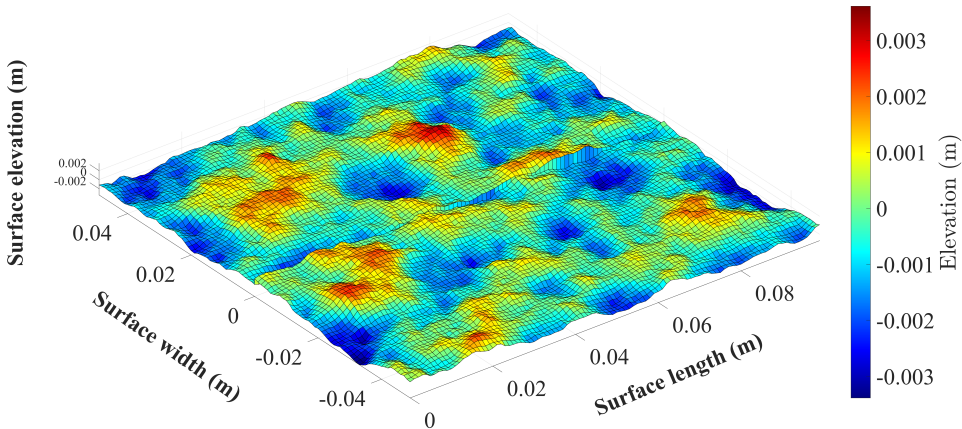


Figure 8. Exemplary base surface of a $0.1 \text{ m} \times 0.1 \text{ m}$ pavement portion with standard deviation $\sigma = 1 \times 10^{-3} \text{ m}$ (e.g., root-mean-square roughness R_q [68]), $H = 0.8$, and a cambered transverse slope of 1 %.

In the next step, design-related irregularities are incorporated into the base surface. The current model version allows for the implementation of longitudinal and transverse slopes, RWY grooving, inset lights like RWY centerline lights, and concrete slabs. Particularly in the touchdown zone (TDZ) of the RWY, rubber abrasion can influence the surface structure by filling the interstices of the macrotexture with rubber particles and thus skid resistance. In our pavement model, this can be simplified by creating the base surface in the touchdown zone area with smoother macrotexture given by values of standard deviation σ and Hurst exponent H . The subsequent insertion of damage patterns requires initially determining the material distinguished into asphalt/flexible or concrete/rigid pavement, and the surface condition rating of the pavement to be modeled. Both parameters influence the type and extent of the implemented damage patterns. Regarding this, the assessment of irregularities/damages, type (e.g., cracks), quantity/frequency (percentage of pavement surface affected by damage), and severity (e.g., depth of a crack) are decisive according to Pavement Condition Index (PCI) [69]. As a first approach for defining quantity and severity of damage patterns in our model, we established a rating scale ranging from *A - excellent* (PCI from 100 - 71), *B - fair* (PCI from 70 - 56) to *C - poor* (PCI from 55 - 0). For these three categories, it was determined based on the pavement material which damages are inserted into the base surface, especially regarding the value ranges of quantity, and severity of each damage pattern. The current model version can depict the damage types specified in Table 1. The ranges of their values were determined based on the information provided in [70, 71, 72] and are summarized exemplarily for different damage types divided into asphalt and concrete pavements in Table 2. Figure 9 presents an exemplary collection of design-related irregularities, illustrated by concrete slabs, and damage patterns of pop-outs, which are incorporated into the modeling approach.

Table 1. Summary of implemented design-related and damage-related irregularities differentiated by pavement materials asphalt and concrete according to [6].

Irregularity	Asphalt (flexible) pavement	Concrete (rigid) pavement
Damage-related	Cracks (general)	Cracks (general)
	Alligator cracking	Map cracking
	Rutting	Corner cracking
	Raveling	Pop-outs
	Heaving	Blowups
	Settlement	Slab settlement
Design-related/operation-related	Inset lights	Joints
	Grooving	Inset lights
	Rubber abrasion (esp. in RWY's touch-down zone)	Grooving
		Rubber abrasion (esp. in RWY's touch-down zone)

The randomized implementation of damage patterns involves determining the starting positions within the underlying grid and defining their extent based on the specified ranges for quantity and severity (cf. Table 2). The principle of randomized determination of damage patterns (index DP) and their characteristics and connected value ranges is explained by the following Equation (14):

$$Z_{DP,r} = Z_{DP,\min} + (Z_{DP,\max} - Z_{DP,\min}) \cdot X \quad \forall X = [0, 1] \quad (14)$$

with $Z_{DP,r}$ randomized damage elevation, $Z_{DP,\min}$ and $Z_{DP,\max}$ are minimum resp. maximum DP elevation in [m] and X a uniformly distributed random number in the interval $[0, 1]$. For an exemplarily concrete surface rated as A (PCI from 100 - 71), and damage pattern of crack (index C), $Z_{DP,\min/\max}$ corresponds to $Z_{C,\min} = 5 \times 10^{-3}$ m and $Z_{C,\max} = 1 \times 10^{-2}$ m. The randomized elevation values for each damage pattern, $Z_{DP,r}$, are iteratively applied to a randomly selected region within the base surface's elevation spectrum $C(q)$, according to Equation (13). This process continues until achieving the specified damage quantity in terms of grid points (cf. Table 2).

$$C(q)_{ij} = C(q)_{ij} + Z_{DP,r_{kl}} \quad (15)$$

This operation applies for $i \in \{sy, sy+1, \dots, ey\}$ and $j \in \{sx, sx+1, \dots, ex\}$, and similarly, $k \in \{dsy, dsy+1, \dots, dey\}$ and $l \in \{dsx, dsx+1, \dots, dex\}$, where sx and ex (resp. sy and ey) denote the randomized start and end grid points on the base surface in the X resp. Y direction. Correspondingly, dsy and dey (resp. dsx and dex) are the start and end points for the damage pattern grid (cf. Figure 7). The final outcome yields a complete elevation profile characterized by length X , width Y , and elevation Z , which can now be integrated into the enriched trajectory (cf. Figure 12).

Due to the inherent grid structure of the model, intricate damage propagation, such as cracks and localized spalling, is approximated using the simplified functional relationships of sine functions, in the current model version. If more precise measurement data on the characteristics of specific damage patterns at an airport are available, it would be possible to refine damage characteristics and create probability density functions (PDF) for damage quantity and severity and incorporate them into the model. Furthermore, in addition to the surface roughness along the entire trajectory,

Table 2. Characteristics overview of exemplary damage patterns based on surface ratings according to [6].

Damage type	Category A	Category B	Category C
Asphalt (flexible) pavement			
Cracks	Quantity: no cracks or cracks with a distance ≤ 30 m Severity: ≤ 3 mm width	Quantity: 15 m distance Severity: 6 mm to 30 mm width	Quantity: 3 m distance Severity: > 30 mm width
Rutting	Quantity: no rutting or $\leq 5\%$ of wheel path Severity: depth ≤ 5 mm	Quantity: 10% to 40% of wheel path Severity: 10 mm to 30 mm depth	Quantity: $\geq 40\%$ of wheel path Severity: ≥ 40 mm depth
Raveling	not existing	Quantity: $\leq 30\%$ per m^2 Severity: ≤ 3 mm depth	Quantity: $> 40\%$ per m^2 Severity: > 3 mm depth
Concrete (rigid) pavement			
Pop-outs	Quantity: $\leq 1\%$ of total surface Severity: ≤ 20 mm diameter, ≤ 13 mm depth	Quantity: 1% to 5% of total surface Severity: ≤ 50 mm diameter, ≤ 20 mm depth	Quantity: 20% to 30% of total surface Severity: ≤ 100 mm diameter, ≥ 20 mm depth
Slab settlement	Quantity: $\leq 5\%$ of all slabs Severity: ≤ 5 mm vertical displacement	Quantity: 8% to 15% of all slabs Severity: 13 mm to 25 mm vertical displacement	Quantity: 8% to 15% of all slabs Severity: > 25 mm vertical displacement
Map cracking	not existing	Quantity: 10% to 20% of total surface Severity: width ≤ 10 mm	Quantity: 30% to 45% of total surface Severity: width ≤ 50 mm

locally restricted surface profiles can be modeled for the analysis of single-event bumps to simulate the occurrence of worst-case load scenarios (limit and ultimate loads according to [7]). In summary, our approach is highly effective for rapidly generating a wide variety of distinct roughness profiles, covering the complete range of possible irregularities, from credible cases to worst-case scenarios.

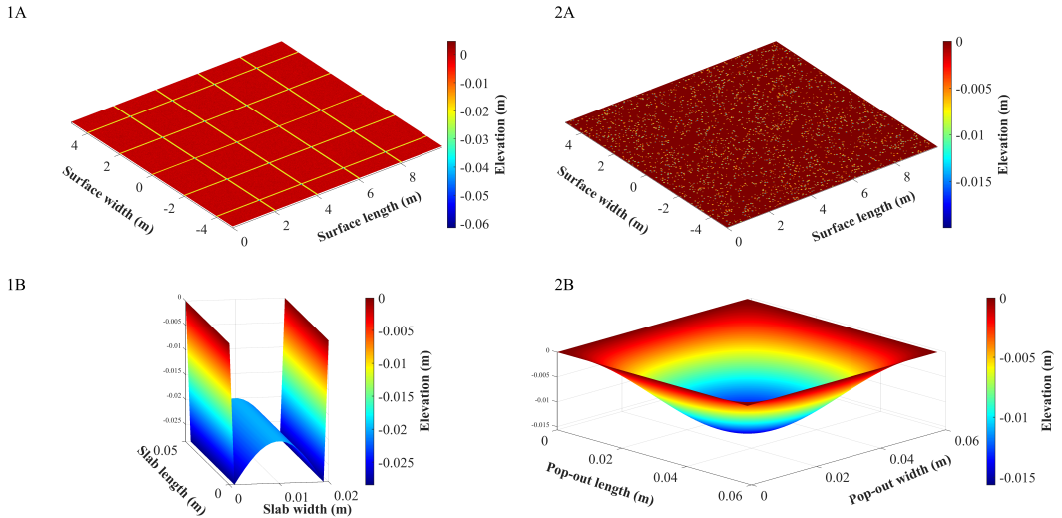


Figure 9. Exemplary design-related irregularity and damage pattern for concrete pavement surface: concrete slabs (1A) and detail view of single slab with filling (1B) as well as pop-out overview (2A) and detail view of single pop-out (2B) according to [6]

3. Application and Results

3.1 Input Data Preparation

For this study, we applied an ADS-B dataset obtained from the OpenSky Network [5]. The dataset only consists of Airbus A220-300 aircraft flight movements at Frankfurt Airport (EDDF) used as reference aircraft type within the load monitor (cf. Figure 1). The dataset spans from May 2019 to June 2022, and contains 649 recorded flight movements. To extract only ground movements, the dataset was initially filtered based on altitude resp. air-ground switch, airport area, and a minimum number of data points per trajectory. As a result, the final dataset contains 291 ground movements, comprising 145 departures and 146 arrivals of aircraft using different RWYs, TWYs, and parking positions (cf. Figure 10). Airport infrastructure data for EDDF was obtained using the *Overpass API* and its front-end, *Overpass Turbo* (<https://overpass-turbo.eu/>). However, due to missing details, the dataset was supplemented with information from the AIP EDDF [73] and AIXM dataset provided by the German Air Navigation Service Provider (ANSP), *DFS Deutsche Flugsicherung GmbH* [74]. The AIXM dataset primarily served for validation and as a source for background mapping in graphical representations.

3.2 Trajectory Modeling

For the application of our map-matching procedure (cf. Section 2.1), the parameters for constructing the graph model must first be defined. We set a proximity threshold of $\epsilon = 3.0$ m according to Equation (2), a distance threshold of $d_{th} = 10.0$ m according to Equation (4), and a search radius of $r_s = 8.0$ m. Adjusting these parameters resulted in more precise outcomes compared to [63] and, consequently, an overall improvement in our map-matching approach. The following Figure 11 shows an extract of the resulting graph model G consisting of nodes and edges.

Building on this, we applied our map-matching approach to all 291 ground movements. Figure 12 presents the corresponding results for one representative sample of ground movement from the

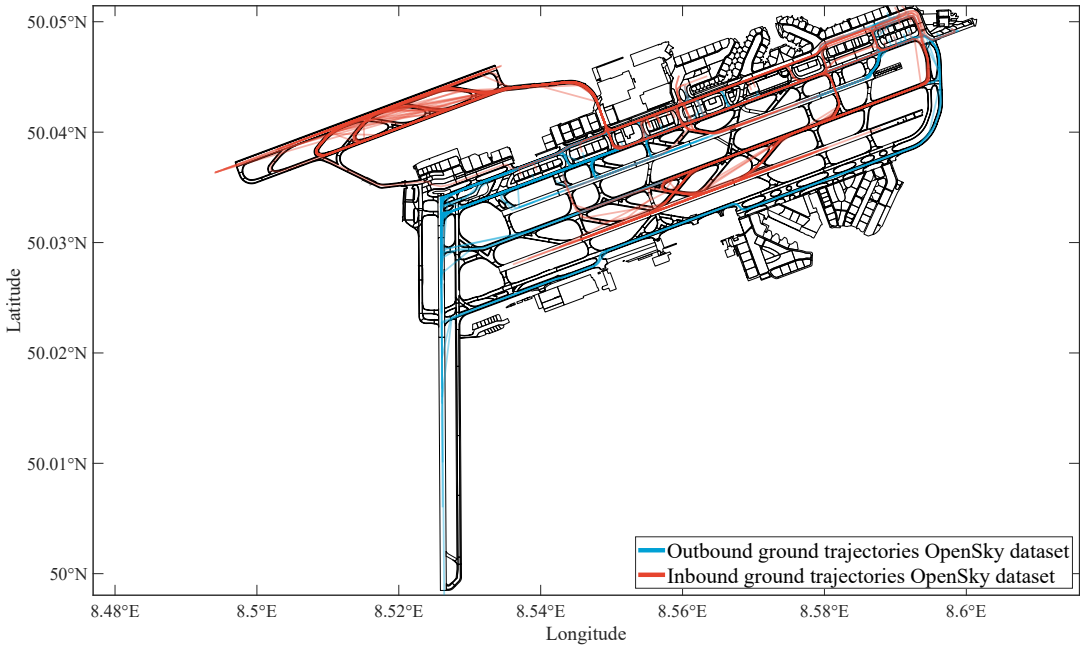


Figure 10. Aircraft ground movements from prefiltered OpenSky Network dataset distinguished into inbound (red) and outbound (blue) traffic summing up to 291 movements at EDDF airport.

dataset, involving a landing on RWY 07R at EDDF airport. The original ADS-B trajectory (red) consists of 151 data points, while the enriched trajectory (blue gradient) now comprises a total of 963 data points, thus demonstrating a significantly improved level of detail and enabling higher mapping accuracy. This improvement is particularly evident in turning segments, such as between RWY 07R and TWY M19, and in the transition from TWY L to TWY N10. However, it should be noted that the algorithm yields inadequate results for 5.5% of the trajectories in the dataset (16 out of 291 samples) and introduces at least minor inaccuracies in 3.8% (11 out of 291 samples) of the analyzed cases. These issues primarily stem from the quality of the ADS-B input data, particularly in instances where large gaps exist between consecutive data points, where erratic patterns occur—especially in ramp areas, notably during pushback—or where position data points deviate from the permissible AOA (cf. Figure 14).

Additionally, we calculated the taxi distances and the average segment speeds along the enriched trajectories, taking into account the relevant considerations as outlined in [63], while also determining the aircraft headings according to Equation (11) as a supplementary analysis. In terms of the total taxi distance, it is observed that the enriched sample trajectory covers approximately 5498 m, while the original ADS-B trajectory only covers approximately 5368 m resulting in an underestimation of about 2.4%. The resulting groundspeeds and headings are presented in Figure 13.

The groundspeed values of 125 m s^{-1} in the original OpenSky Network [5] ADS-B dataset for the sample ground trajectory shown in Figure 13 should be considered unrealistic, likely representing the last reliable speed measurement. These values were presumably propagated to the remaining data points on the ground. The average segment speeds in Figure 13 were calculated by determining the distance and time between adjacent ADS-B points from the OpenSky Network [5] dataset, as detailed in [63]. Data points filled via map-matching were excluded, as interpolated timestamps may not accurately reflect the aircraft's actual movement. Further analysis revealed that within the ground distance range of approximately 1000 m to 3000 m, distances between adjacent ADS-B data

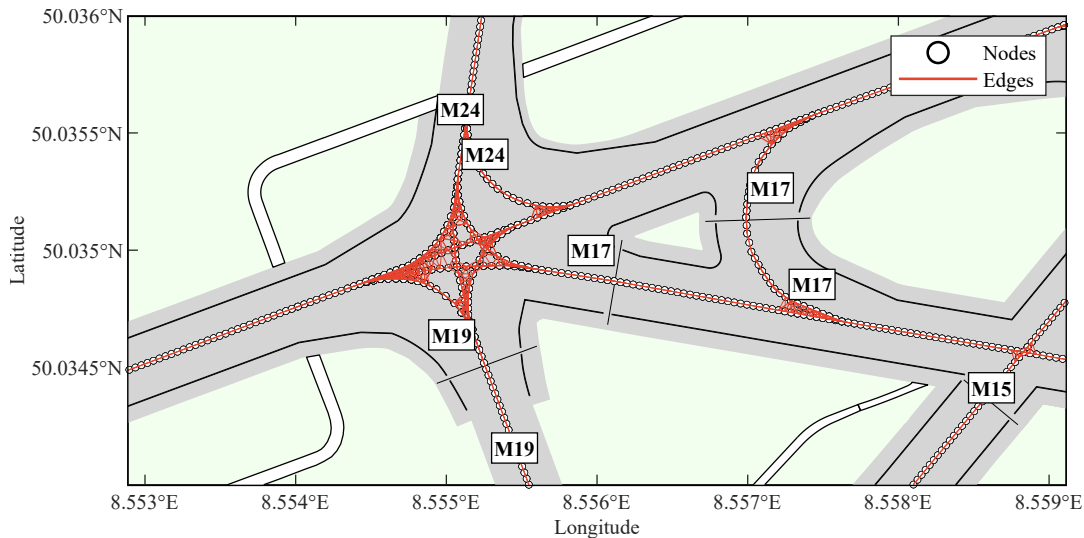


Figure 11. Excerpt of the graph model showing nodes and edges including TWY designators.

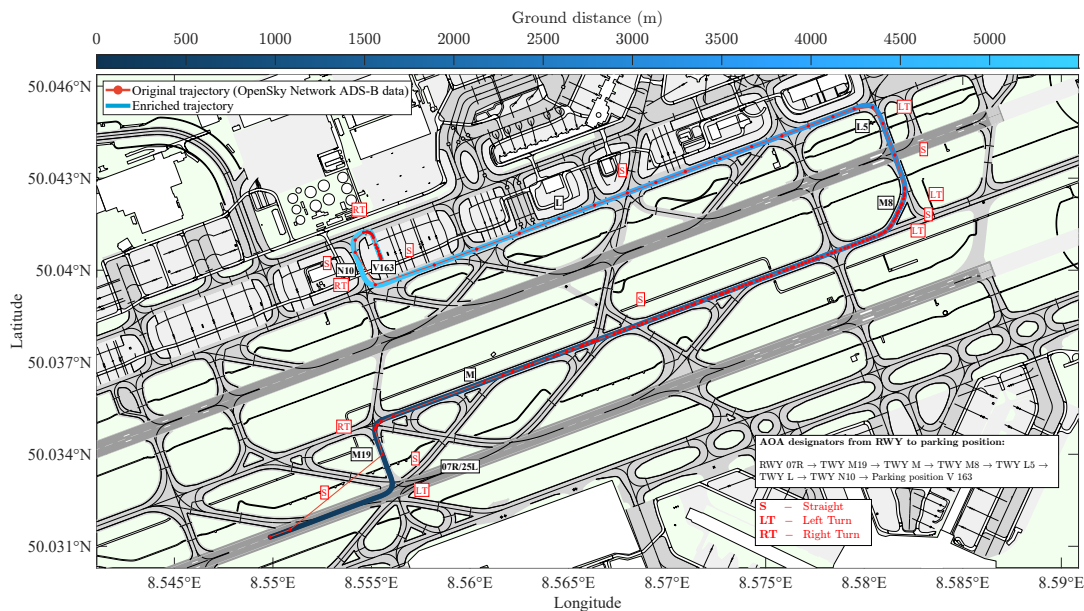


Figure 12. Algorithmically enriched ground trajectory of a sample flight, with ground distance-based color coding. The original OpenSky Network [5] positions (red) and the resulting enriched trajectory are shown. AOA designators from the RWY to the final parking position were automatically determined and are summarized in the white textbox. Segmentation results, derived in accordance with Equation (12), are displayed in the red textboxes.

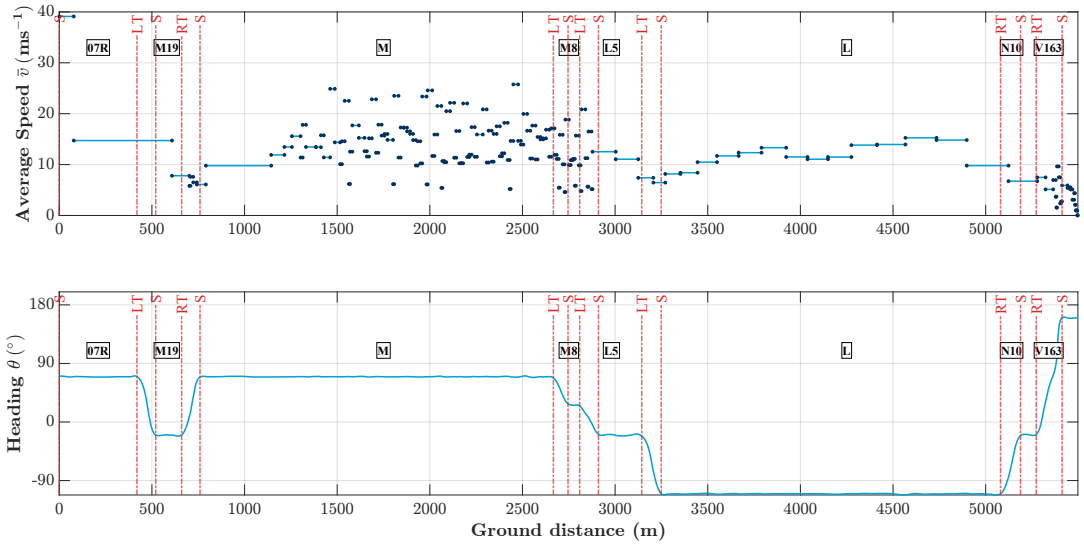


Figure 13. Average segment speeds (top) and headings (bottom) over ground distance for the sample flight, as shown in Figure 12. The red vertical dashed lines indicate the transitions between different trajectory segments: straights (S), left turns (LT), and right turns (RT). The black textboxes display the corresponding AOA designators.

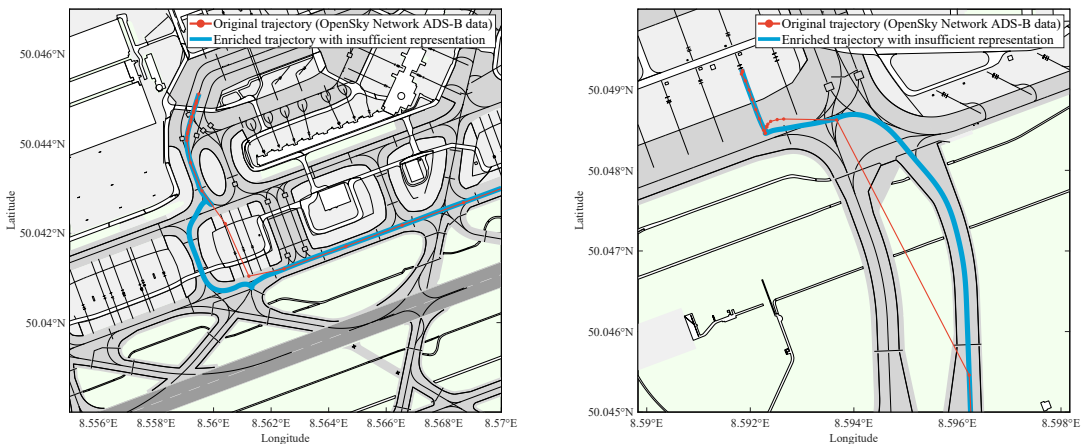


Figure 14. ADS-B data from OpenSky Network [5] (red) and the enriched trajectory (blue) are shown for two sample flights. Left (inbound): Deviations from the actual taxi path or shortcuts over parking positions likely cause inconsistencies. Right (outbound): Imprecise enriched trajectory representation during pushback due to the absence of specific ground markings, limiting map-matching accuracy.

points vary (around 5 m to 25 m), while time intervals remain relatively constant at about 1 s. This discrepancy leads to fluctuating groundspeed values, suggesting imprecise timestamps.

The calculated headings in Figure 13 are represented within a range of $+180^\circ$ to -180° , where negative values correspond to angles between 180° and 360° . This representation is preferable over a 0° to 360° scale as it ensures continuity when crossing the $0^\circ/360^\circ$ threshold, thereby avoiding abrupt numerical jumps. The derived heading values using Equation (11) effectively capture the directional changes within the trajectory segments, aligning well with the transitions between straights and turns. Additionally, these headings provide input for estimating steering angles in our aircraft motion model (cf. Figure 1) by applying the following Equation (16):

$$\delta = \text{atan} \left(\frac{\dot{\Phi} \cdot l}{v} \right) \quad (16)$$

Here, δ represents the steering angle in degrees ($^\circ$), $\dot{\Phi}$ denotes the rate of change of the heading over time, corresponding to the yaw rate in degrees per second ($^\circ \text{ s}^{-1}$). The parameter l is the distance between the aircraft's nose landing gear and the main landing gear, given in meters (m), and v corresponds to the aircraft speed in meters per second (m s^{-1}). The application of Equation (16) highlights the critical importance of accurate velocity data and precise timestamps in determining valid steering angles.

To evaluate the enriched ground trajectory, its calculated taxi distances are compared with the distances derived from OpenSky Network [5] ADS-B position data. Additionally, the estimated segment speeds of the enriched trajectory—computed based on these ADS-B distances—are contrasted with the speeds obtained from the enriched trajectory's total taxi distances. These discrepancies, which arise due to differences in the assumed taxiing path and the corresponding speed estimation, are referred to as distance error and speed error in the following analysis. In [63], these distance and speed errors were analyzed across a dataset of 291 ground movements. However, this analysis included the aforementioned faulty and imprecise samples. Since these can distort the results—for example, when the enriched trajectory produces diversions, as depicted in Figure 14 (left)—a total of 27 samples were excluded from the analysis. The distance error was calculated using the following Equation (17):

$$\begin{aligned} \text{Distance Error}_i &= d_{f,i,i+1} - d'_{f,i,i+1} \\ d_{f,i,i+1} &= \sqrt{(x_{f,i} - x_{f,i+1})^2 + (y_{f,i} - y_{f,i+1})^2} \end{aligned} \quad (17)$$

Additionally, the speed error was computed using the following Equation (18):

$$\begin{aligned} \text{Speed Error}_i &= v_{f,i,i+1} - v'_{f,i,i+1} \\ v_{f,i,i+1} &= \frac{d_{f,i,i+1}}{t_{f,i+1} - t_{f,i}} \end{aligned} \quad (18)$$

Figure 15 illustrates the distribution of distance errors (left) and speed errors (right) throughout the dataset, excluding faulty enriched trajectories. Negative distance errors indicate that the direct distance between two ADS-B measurements is shorter than the actual taxi distance derived from the enriched trajectory. The majority of errors remain relatively small, within 0 m to -5 m, but some notable deviations occur, reaching up to -100 m. Specifically, extreme distance errors in the range of -100 m to -80 m occur with a frequency of approximately 5.50×10^{-5} , whereas errors between -20 m to -10 m are observed at a frequency of about 3.90×10^{-3} . Similarly, negative speed errors indicate an underestimation of ground speed, which is closely related to an underestimated taxi distance between successive ADS-B data points. While most speed errors remain within 0 m s^{-1} to -5 m s^{-1} ,

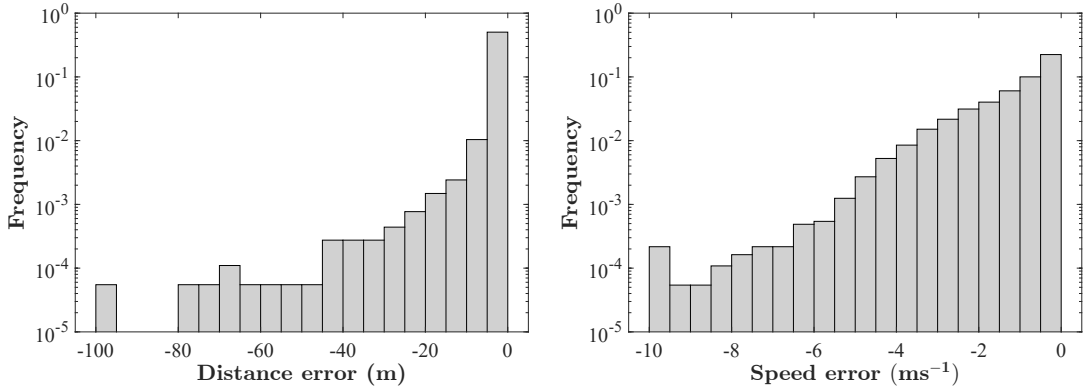


Figure 15. Histograms showing the distributions of distance (left) and speed (right) errors as per Equation (17) resp. Equation (18): The distances between consecutive ADS-B data points are lower than those of the enriched trajectory data points. Due to the underestimation of distances, the speeds calculated between consecutive ADS-B data points are also lower than the actual values.

larger discrepancies of up to -10 m s^{-1} are observed. The frequency of underestimations in the range of -10 m s^{-1} to -8 m s^{-1} is approximately 4.34×10^{-4} , whereas errors between -2 m s^{-1} to -1 m s^{-1} occur with a significantly higher frequency of about 1.01×10^{-1} . These findings demonstrate that most distance and speed errors are small, but significant outliers indicate underestimation, particularly in curve segments. These deviations highlight that the trajectories from sparse ADS-B data underestimate the actual distances and speeds, with the enriched trajectory providing a more accurate and realistic representation of the true ground trajectory.

3.3 Pavement Roughness Modeling

Building on the analysis of the sample ground trajectory (cf. Figure 12), particularly in terms of ground distances and AOA designators, along with information from AIP EDDF [73] supplemented by AIXM [74], the input data for pavement modeling is further refined. EDDF pavements are rated A (PCI from 100 - 71), indicating compliance with EASA guidelines (esp. condition and maintenance status of pavements). The base surface has a standard deviation $\sigma = 1 \times 10^{-3} \text{ m}$ and Hurst exponent $H = 0.8$. For the mentioned sample trajectory, design-related irregularities and damage patterns can be generated in four sections with different characteristics summarized in Table 3:

Table 3. Overview of pavement section characteristics applied for roughness modeling.

Section	AOA Designator	Length X (m)	Width Y (m)	Pavement Material	Longitudinal Slope (%)	Transverse Slope (%)	Lighting
1 st	RWY 07R (portion)	450.0 m	10.0 m	Asphalt	0.3	1.0	Centerline (spacing: 15 m)
2 nd	TWY M19	280.0 m	10.0 m	Concrete	0.0	0.0	None
3 rd	TWY M to TWY N10	4600.0 m	10.0 m	Asphalt	0.0	0.0	Centerline (spacing: 15 m)
4 th	Parking position V163	100.0 m	10.0 m	Concrete	0.0	0.0	None

According to Table 3, the modeled surface width for all four sections aligns with the Airbus A220-300 main landing gear width of 6.7 m, including buffers, and is set to $Y = 10 \text{ m}$ for modeling purposes. In-

formation regarding surface lighting, pavement materials, and slopes is derived from AIP EDDF [73] and AIXM [74]. The spacing of TWY centerline lights varies, particularly between curved sections and straight segments, and is further influenced by holding position lights, stop bars, and other lighting elements, which are not included in this analysis. TWY M19 and the apron area in the vicinity of parking position V163 are not equipped with centerline lights. Additional details on position and spacing can be obtained from AIXM [74]. However, no data on the longitudinal and transverse slopes of the TWY are available. Furthermore, grooving and rubber abrasion are not considered due to the lack of reliable data. Figure 16 presents the results of the surface roughness modeling following the methodology outlined in Chapter 2.2 and applying the aforementioned pavement characteristics.

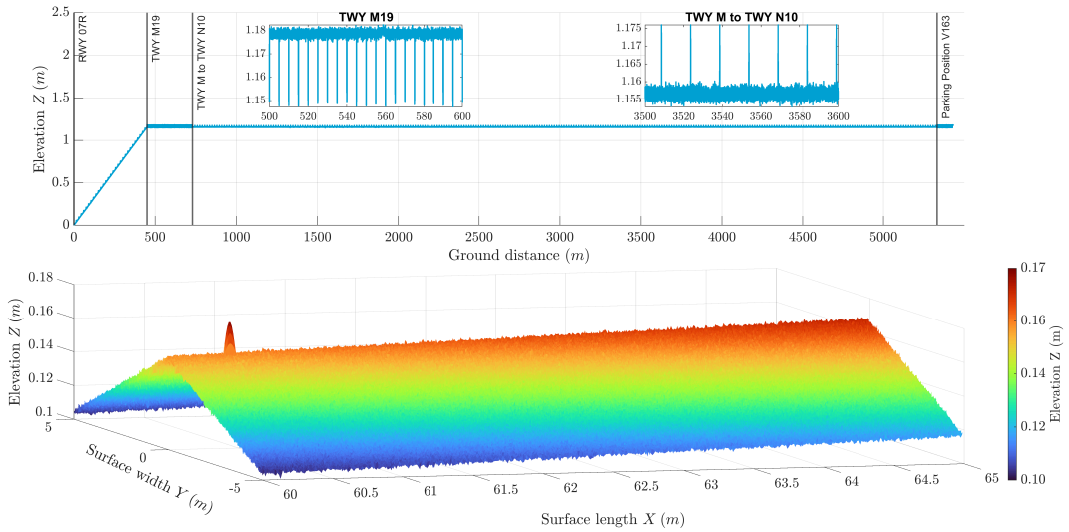


Figure 16. Modeled pavement profile along the sample trajectory. The upper figure shows the surface profile along the centerlines, with detailed views of TWY M19 (concrete pavement) and TWY M to N10 (asphalt pavement). The lower figure illustrates the detailed 3D roughness along RWY 07R, featuring a cambered surface. The peak on the left represents a RWY inset centerline light. Note: The Z-axes are exaggerated, making the longitudinal and transverse slopes appear steeper.

In the upper subplot of Figure 16, the centerline profile along the modeled ground trajectory is presented, corresponding to the four sections defined in Table 3. The left detail view highlights the TWY M19 area, which has a concrete surface. The vertical lines in the profile represent the concrete joints, spaced at 5 m intervals. The right detail view illustrates the asphalt surface in the section between TWY M and TWY N10, where the centerline inset lights are visible in the profile, positioned at 15 m intervals. Additionally, the lower subplot presents a section of the modeled 3D pavement profile of RWY 07R between 60 m to 65 m, representing the stochastic pavement roughness. In addition to the longitudinal slope of 0.3 %, the transverse slope of 1.0 % is clearly visible on both sides of the RWY centerline, featuring a cambered surface where the transverse slope is symmetrical on both sides of the centerline, a standard design for RWYs as defined by EASA [39]. On the left side of the subplot, the peak represents a RWY centerline inset light. The generated stochastic pavement roughness profiles must be compared with actual measured RWY and TWY profiles for validation purposes, for instance, those provided by pavement analysis software *ProFAA* [41], particularly in terms of frequency components relevant to aircraft taxiing dynamics. The influence of different roughness profiles and irregularities on aircraft landing gear dynamics, specifically in the form of vertical accelerations and structural loads, must be assessed within our aircraft motion model as part of the load monitor (cf. Figure 1), which is a key focus of future investigations (cf. Chapter 4).

In summary, the integration of our trajectory model (cf. Chapter 2.1) with the pavement roughness model (cf. Chapter 2.2) provides a methodology for generating high-fidelity 4D ground trajectories. These trajectories serve as critical input data for our aircraft motion model within the framework of the load monitor (cf. Figure 1).

4. Conclusion and Outlook

This paper contributes to advancing the development of a landing gear load monitor within a digital twin framework, aimed at modeling the forces and moments produced during aircraft ground operations. For this purpose, we developed a methodology enabling highly automated generation of 4D trajectories using exclusively open-source data. Utilizing the methodology outlined in our study, we demonstrated the feasibility of accurately reconstructing aircraft ground trajectories. This is achieved through the integration of sparse ADS-B position data and geospatial airport information sourced from OSM, alongside the consistent application of map-matching techniques utilizing open-source data. Employing filtering techniques enhances the accuracy of trajectory determination, surpassing the limitations of raw ADS-B data. Moreover, our methodology facilitates comprehensive analysis of enriched trajectories, including parameters such as ground speed, heading, allocation of AOA designators, and segmentation of trajectories into distinct turning and straight segments.

Additionally, we developed a methodology that allows for stochastically modeling of surface roughness profiles based on PSD method and integrates typical design-related irregularities as well as damage patterns for asphalt and concrete. The damage patterns vary in terms of quantity and severity according to a developed rating scale. This modeling approach also relies entirely on open-source data.

Opportunities exist for enhancing the preprocessing of OSM data, specifically regarding the accurate integration of AOA designators as per the AIP. Moreover, in OSM data, the positions denoted by AOA centerlines, particularly in densely marked airport zones, e.g., TWY intersections or apron taxi lanes, may occasionally overlap, posing challenges in augmenting trajectory data with precise data points. An improvement could be achieved by incorporating AIXM data [74] as an alternative, which provide highly accurate information on markings, surface lighting, and designators, reflecting the actual conditions at the respective airport. This integration could further enhance the accuracy and overall quality of our map-matching approach. Furthermore, the pavement model can be refined, particularly regarding the adjustment of the input coefficients used in [68], differentiated for rigid and flexible pavements, for instance, through surveys.

Future work involves validating our model through several potential methods. One approach could be to compare smoothed trajectories from sparse ADS-B data against data derived from Flight Data Monitoring systems using inertial navigation system (INS) to assess deviations between modeled and actual positions. Another validation approach would involve utilizing an ADS-B dataset that provides a representation of a surface trajectory with high data quality (e.g., Zurich Airport) or applying trajectories derived from more precise Airport Surface Detection Equipment, Model X (ASDE-X) data. Segments of the resulting trajectory from more precise data records could then be removed, after which our map-matching approach would be applied, and the delta between the original trajectory and the enriched trajectory would be determined.

Regarding pavement roughness, a possibility is to compare the modeled roughness profiles to profiles from real RWY and TWY, for example provided by *ProFAA*, by calculating various pavement indexes. Furthermore, calculating vertical accelerations from modeled roughness profiles using an aircraft motion model and compare these to typical values from other studies (e.g., [49]) and real measurements from aircraft INS or external measurement systems like inertial profilers is suitable. However, it's important to note that barometric and GNSS altitude values as well as ground speed

values during taxi derived from OpenSky Network ADS-B data [5] currently have limitations due to their low resolution and accuracy and are not appropriate for validation purposes.

Subsequently, the modeled trajectories will be incorporated into the motion model (cf. Figure 1). This integration will facilitate the interpolation of trajectory segments between ADS-B data points, incorporating realistic speed and acceleration profiles. Furthermore, it will allow for the evaluation of landing gear loads under different operational conditions. Further investigations are required in this regard. For example, a comparison of the level of detail of the surface roughness with the tire model needs to be conducted, taking into account the representation of vibrations within the frequency range of the tire model.

Author contributions

- Martin Schlosser: Conceptualization, Methodology, Software, Validation, Formal Analysis, Investigation, Resources, Writing (Original Draft), Writing (Editing), Visualization
- Hannes Braßel: Conceptualization, Methodology, Software, Validation, Formal Analysis, Investigation, Resources, Writing (Original Draft), Writing (Review and Editing), Visualization
- Hartmut Fricke: Resources, Writing (Review), Supervision

Open data statement

The ADS-B data set used in this study is freely available on the OpenSky Network website <https://opensky-network.org/>. Based on OpenStreetMap (OSM) information, infrastructure data for map-matching can be accessed for numerous international airports via the Overpass API <https://overpass-api.de/>, its associated Overpass Turbo front-end <https://overpass-turbo.eu/> or via AIXM <https://aixm.aero/> resp. <https://aip.dfs.de/datasets/>.

Reproducibility statement

Source code, input data and figures are available on the following GitLab repository: <https://tud.link/s5sx4z>.

References

- [1] M. Liao, G. Renaud, and Y. Bombardier. “Digital Twin Technology Development and Demonstration for Aircraft Structural Life-cycle Management”. In: *Proc. SPIE 12489, NDE 4.0, Predictive Maintenance, Communication, and Energy Systems: The Digital Transformation of NDE*. 2023, p. 1248906. DOI: 10.1117/12.2662879.
- [2] C. Delprete, A. Dagna, and E. Brusa. “Model-Based Design of Aircraft Landing Gear System.” In: *Appl. Sci.* 13 (2023), p. 11465. DOI: 10.3390/app132011465.
- [3] S. Heim, J. Clemens, J. E. Steck, C. Basic, D. Timmons, and K. Zwiener. “Predictive Maintenance on Aircraft and Applications with Digital Twin”. In: *2020 IEEE International Conference on Big Data (Big Data)*. Atlanta, GA, USA, 2020, pp. 4122–4127. DOI: 10.1109/BigData50022.2020.9378433.
- [4] M. Xiong and H. Wang. “Digital twin applications in aviation industry: A review.” In: *Int J Adv Manuf Technol* 121 (2022), pp. 5677–5692. DOI: 10.1007/s00170-022-09717-9.
- [5] M. Schäfer, M. Strohmeier, V. Lenders, I. Martinovic, and M. Wilhelm. “Bringing up OpenSky: A large-scale ADS-B sensor network for research”. In: *Proceedings of the 13th international symposium on Information processing in sensor networks*. 2014, pp. 83–94.
- [6] E. T. Schulz. *Modeling of Airport Surface Profiles for Determining Aircraft Landing Gear Loads*. Diploma thesis, TUD Dresden University of Technology. 2022.
- [7] European Union Aviation Safety Agency (EASA). *Certification Specifications and Acceptable Means of Compliance for Large Aeroplanes (CS-25)*. Annex to ED Decision 2023/021/R, Amendment 28. 2023.

- [8] C. C. Tung, J. Penzien, and R. Horonjeff. *The Effect of Runway Unevenness on the Dynamic Response of Supersonic Transports*. NASA Contractor Report CR-119, University of California. 1964.
- [9] Shifu Liu, Jianming Ling, Yu Tian, and Jinsong Qian. “Assessment of aircraft landing gear cumulative stroke to develop a new runway roughness evaluation index”. In: *International Journal of Pavement Engineering* 23.10 (2021), pp. 3609–3620. doi: 10.1080/10298436.2021.1910823.
- [10] G. J. Morris A. W. Hall P. A. Hunter. “Recent Studies of Runway Roughness.” In: *NASA Aircraft Safety and Operating Problems 1*, NASA SP-270 (1971), pp. 127–142.
- [11] Federal Aviation Administration (FAA). *Advisory Circular 150/5320-9: Guidelines and Procedures for Measuring Airfield Pavement Roughness*. 2009.
- [12] Jorge Braulio Cossío Durán and José Leomar Fernandes Júnior. “Airport pavement roughness evaluation based on cockpit and center of gravity vertical accelerations”. In: *TRANSPORTES* 28.1 (2020), pp. 147–159. doi: 10.14295/transportes.v28i1.1932. URL: <https://www.revistatransportes.org.br/anpet/article/view/1932>.
- [13] Guizhang Hu, Peigen Li, Haiting Xia, Tao Xie, Yifan Mu, and Rongxin Guo. “Study of the Dynamic Response of a Rigid Runway with Different Void States during Aircraft Taxiing”. In: *Applied Sciences* 12.15 (2022). ISSN: 2076-3417. doi: 10.3390/app12157465. URL: <https://www.mdpi.com/2076-3417/12/15/7465>.
- [14] Federal Aviation Administration (FAA). *Advisory Circular 25.491-1: Taxi, Takeoff and Landing Roll Design Loads*. 2000.
- [15] M. M. Kanafi and A. Tuononen. “Application of three-dimensional printing to pavement texture effects on rubber friction.” In: *Road Materials and Pavement Design* 18.4 (2017), pp. 865–881. doi: 10.1080/14680629.2016.1194883.
- [16] European Union Aviation Safety Agency (EASA). *Acceptable Means of Compliance (AMC) and Guidance Material (GM) to Part-CAT*. Annex III to ED Decision 2023/007/R, Issue 2, Amendment 23. 2023.
- [17] R. Dalmau, X. Prats, and A. Ramonjoan. “Estimating Fuel Consumption from Radar Tracks: A Validation Exercise Using FDR and Radar Tracks from Descent Trajectories”. In: *CEAS Aeronaut J* 11 (2020), pp. 355–365. doi: 10.1007/s13272-020-00441-2.
- [18] T.-N. Tran, D.-T. Pham, and S. Alam. “A Map-Matching Algorithm for Ground Movement Trajectory Representation using A-SMGCS Data”. In: *2020 International Conference on Artificial Intelligence and Data Analytics for Air Transportation (AIDA-AT)*. Singapore, 2020, pp. 1–8. doi: 10.1109/AIDA-AT48540.2020.9049181.
- [19] Federal Aviation Administration (FAA). *Airport Surface Detection Equipment, Model X (ASDE-X)*. Available online at https://www.faa.gov/air_traffic/technology/asde-x. 2024.
- [20] M. Schultz, X. Olive, J. Rosenow, H. Fricke, and S. Alam. “Analysis of airport ground operations based on ADS-B data”. In: *International Conference on Artificial Intelligence and Data Analytics for Air Transportation (AIDA-AT)*. Singapore, 2020, pp. 1–9. doi: 10.1109/AIDA-AT48540.2020.9049212.
- [21] J. Hoole, P. Sartor, J.D. Booker, J.E. Cooper, X.V. Gogouvitis, and R.K. Schmidt. “Landing gear ground manoeuvre statistics from automatic dependent surveillance-broadcast transponder data”. In: *The Aeronautical Journal* 125.1293 (2021), pp. 1942–1976. doi: 10.1017/aer.2021.45.
- [22] L. Basora, X. Olive, and T. Dubot. “Recent Advances in Anomaly Detection Methods Applied to Aviation”. In: *Aerospace* 6.11 (2019), p. 117. doi: 10.3390/aerospace6110117.
- [23] X. Olive, J. Grignard, T. Dubot, and J. Saint-Lot. “Detecting controllers’ actions in past Mode S data by autoencoder-based anomaly detection”. In: *8th SESAR Innovation Days*. 2018.
- [24] X. Tang, X. Ji, and J. Liu. “Predicting Aircraft Taxiing Estimated Time of Arrival by Cluster Analysis”. In: *IET Intell. Transp. Syst.* 16 (2022), pp. 252–262. doi: 10.1049/itr2.12141.
- [25] M. K. El Mahrsi, C. Andrieu, E. Côme, Z. Bezza, L. Oukhellou, and F. Rossi. “Traffic Characterization on Airport Surface Using Aircraft Ground Trajectories”. In: *2018 21st International Conference on Intelligent Transportation Systems (ITSC)*. Maui, HI, USA, 2018, pp. 3879–3885. doi: 10.1109/ITSC.2018.8569350.
- [26] A. M. Churchill and M. Bloem. “Clustering Aircraft Trajectories on the Airport Surface”. In: *Proceedings of the 13th USA/Europe Air Traffic Management Research and Development Seminar*. Chicago, IL, USA, 2019.
- [27] R. E. Bach and R. A. Paielli. *A User Guide for Smoothing Air Traffic Radar Data*. NASA/TM 2014–216520. NASA Ames Research Center, 2014.
- [28] J. D. Giovino. “Idealized Truth Data for System Modeling and Testing”. In: *2008 Integrated Communications, Navigation and Surveillance Conference*. IEEE. 2008, pp. 1–10.

- [29] H. Khadilkar and H. Balakrishnan. "A multi-modal unscented Kalman filter for inference of aircraft position and taxi mode from surface surveillance data". In: *Proceedings of the 11th AIAA Aviation Technology, Integration, and Operations (ATIO) Conference*. 2011. DOI: 10.2514/6.2011-7051.
- [30] Xavier Olive, Manuel Waltert, Ryota Mori, and Philippe Mouyon. "Filtering Aircraft Surface Trajectories Using Information on the Taxiway Structure of Airports". In: *11th International Conference on Research in Air Transportation (ICRAT)*. https://www.researchgate.net/publication/382143178_Filtering_Aircraft_Surface_Trajectories_Using_Information_on_the_Taxiway_Structure_of_Airports. Singapore, July 2024.
- [31] E. Mazor, A. Averbuch, Y. Bar-Shalom, and J. Dayan. "Interacting Multiple Model Methods In Target Tracking: A Survey". In: *IEEE Transactions On Aerospace And Electronic Systems* 34.1 (1998), pp. 103–123.
- [32] G. W. Pulford. "A Survey of Manoeuvring Target Tracking Methods". In: *arXiv preprint arXiv:1503.07828* (2015).
- [33] M. Vogel, C. Thiel, H. Fricke, M. Lindner, and Federal Environmental Agency (UBA). *Flight trajectory data as a basis for aircraft noise calculations*. Final Report (in German), Texte 22/2022. <https://www.umweltbundesamt.de/publikationen/flugverlaufsdaten-als-grundlage-fuer>. 2022.
- [34] M. Tortora, E. Cordelli, and P. Soda. "PyTrack: A Map-Matching-Based Python Toolbox for Vehicle Trajectory Reconstruction". In: *IEEE Access* 10 (2022), pp. 112713–112720. DOI: 10.1109/ACCESS.2022.3216565.
- [35] Z. Gao, X. Zhang, M. Zhang, Y. Yang, and K. Cai. "A Novel Semantic Representation of Airport Surface Trajectory for Taxiing Pattern Recognition". In: *2023 IEEE/AIAA 42nd Digital Avionics Systems Conference (DASC)*. Barcelona, Spain, 2023, pp. 1–10. DOI: 10.1109/DASC58513.2023.10311315.
- [36] X. Wang, A. E. I. Brownlee, M. Weiszer, J. R. Woodward, M. Mahfouf, and J. Chen. "An Interval Type-2 Fuzzy Logic-Based Map Matching Algorithm for Airport Ground Movements". In: *IEEE Transactions on Fuzzy Systems* 31.2 (2023), pp. 582–595. DOI: 10.1109/TFUZZ.2022.3221793.
- [37] M. A. Quddus, W. Y. Ochieng, and R. B. Noland. "Current map-matching algorithms for transport applications: State-of-the art and future research directions". In: *Transp. Res. Part C: Emerg. Technol.* 15.5 (2007), pp. 312–328. DOI: 10.1016/j.trc.2007.05.002.
- [38] M. Hashemi and H. A. Karimi. "A critical review of real-time map-matching algorithms: Current issues and future directions". In: *Comput. Environ. Urban Syst.* 48 (2014), pp. 153–165. DOI: 10.1016/j.compenvurbsys.2014.07.004.
- [39] European Union Aviation Safety Agency (EASA). *Easy Access Rules for Aerodromes Regulation (EU) No 139/2014*. Available online at <https://www.easa.europa.eu/en/downloads/98016/en>. 2024.
- [40] European Union Aviation Safety Agency (EASA). *Acceptable Means of Compliance (AMC) and Guidance Material (GM) to Authority, Organisation and Operations Requirements for Aerodromes*. Annex V to ED Decision 2023/010/R, Issue 1, Amendment 9. Available online at <https://www.easa.europa.eu/en/regulations/aerodromes-adr>. 2023.
- [41] Federal Aviation Administration (FAA). *Airport Pavement*. <https://www.airporttech.tc.faa.gov/Airport-Pavement> [Accessed: May 2024]. 2024.
- [42] US Army Corps of Engineers (USACE). *Assessment of LiDAR- and Photogrammetry-based Airfield Roughness Profiling Techniques*. Final Report, ERDC TR-19-11. 2019.
- [43] Federal Aviation Administration (FAA). *Practical Lessons Learned from Planning, Collecting, Processing, and Analyzing Small Unmanned Aircraft System Data for Airfield Pavement Inspection*. Final Report, DOT/FAA/TC-22/48. 2022.
- [44] Federal Aviation Administration (FAA). *Small Unmanned Aircraft System for Pavement Inspection*. Final Report, DOT/FAA/TC-23/50. 2023.
- [45] Ahmad Alhasan, Kyle Younkin, and David White. *Comparison of Roadway Roughness Derived from Lidar and SFM 3D Point Clouds*. Center for Earthworks Engineering and Research, Iowa State University. 2015.
- [46] E. L. Gervais. "Runway Roughness Measurement, Quantification and Application: the Boeing Approach". In: *Aircraft/Pavement Interaction; An Integrated System* (1991), pp. 121–131.
- [47] ASTM International. *Standard Practice for Computing International Roughness Index of Roads from Longitudinal Profile Measurements*. E1926–08. 2021. DOI: 10.1520/E1926â€08R21.
- [48] ASTM International. *Standard Test Method for Airport Pavement Condition Index Surveys*. D5340:23. 2023. DOI: 10.1520/D5340-23.
- [49] Federal Aviation Administration (FAA). *Boeing 737-800 Final Surface Roughness Study Data Collection*. Final Report, DOT/FAA/TC-18/8. 2017.

- [50] Federal Aviation Administration (FAA). *Development of New Roughness Standards for In-Service Airport Pavement*. Final Report, DOT/FAA/TC-21/39. 2021.
- [51] Shifu Liu, Yu Tian, Le Liu, Peng Xiang, and Zhekai Zhang. “Improvement of Boeing Bump Method Considering Aircraft Vibration Superposition Effect”. In: *Applied Sciences* (2021). doi: 10.3390/app11052147.
- [52] Mona Mahboob Kanafi, Antti Kuosmanen, Terhi K Pellinen, and Ari Juhani Tuononen. “Macro- and micro-texture evolution of road pavements and correlation with friction”. In: *International Journal of Pavement Engineering* 16.2 (2015), pp. 168–179. doi: 10.1080/10298436.2014.937715.
- [53] Mona Mahboob Kanafi, Ari Juhani Tuononen, Leonid Dorogin, and Bo NJ Persson. “Rubber friction on 3D-printed randomly rough surfaces at low and high sliding speeds”. In: *Wear* 376-377 (2017). 21st International Conference on Wear of Materials, pp. 1200–1206. issn: 0043-1648. doi: <https://doi.org/10.1016/j.wear.2017.01.092>. url: <https://www.sciencedirect.com/science/article/pii/S0043164817302235>.
- [54] Mona Mahboob Kanafi and Ari Juhani Tuononen. “Top topography surface roughness power spectrum for pavement friction evaluation”. In: *Tribology International* 107 (2017), pp. 240–249. issn: 0301-679X. doi: <https://doi.org/10.1016/j.triboint.2016.11.038>. url: <https://www.sciencedirect.com/science/article/pii/S0301679X16304674>.
- [55] Anle Wang and Martin H. Müser. “On the adhesion between thin sheets and randomly rough surfaces”. In: *Frontiers in Mechanical Engineering* (2022). doi: 10.3389/fmech.2022.965584.
- [56] Arun Majumdar, Arun Majumdar, C. L. Tien, and C.L. Tien. “Fractal characterization and simulation of rough surfaces”. In: *Wear* 136 (2 1990), pp. 313–327. doi: 10.1016/0043-1648(90)90154-3.
- [57] Bo Persson. “On the Fractal Dimension of Rough Surfaces”. In: *Fundamentals of Friction and Wear on the Nanoscale*. Ed. by Enrico Gnecco and Ernst Meyer. Cham: Springer International Publishing, 2015, pp. 235–248. isbn: 978-3-319-10560-4. doi: 10.1007/978-3-319-10560-4_12. url: https://doi.org/10.1007/978-3-319-10560-4_12.
- [58] Tevis D B Jacobs, Till Junge, and Lars Pastewka. “Quantitative characterization of surface topography using spectral analysis”. In: *Surface Topography: Metrology and Properties* 5.1 (Jan. 2017), p. 013001. doi: 10.1088/2051-672X/aa51f8. url: <https://dx.doi.org/10.1088/2051-672X/aa51f8>.
- [59] Van-Hieu Nguyen, Duy-Dong Nguyen, and Vladimir Tatarinov. “Methods of spectral density estimation for airfield pavements”. In: *MATEC Web of Conferences* 251 (Jan. 2018), p. 04002. doi: 10.1051/mateconf/201825104002.
- [60] J. Qian, Y. Cen, X. Pan, Y. Tian, and S. Liu. “Spectrum parameters for runway roughness based on statistical and vibration analysis”. In: *International Journal of Pavement Engineering* 23.11 (2022), pp. 3757–3769. doi: 10.1080/10298436.2021.1916821.
- [61] C. L. Kirk and P. J. Perry. “Analysis of Taxiing Induced Vibrations in Aircraft by the Power Spectral Density Method”. In: *The Aeronautical Journal* 75.723 (1971), pp. 182–194. doi: 10.1017/S0001924000045097.
- [62] European Union Aviation Safety Agency (EASA). *Certification Specifications and Acceptable Means of Compliance for Airborne Communications, Navigation and Surveillance (CS-ACNS)*. Annex to ED Decision 2022/008/R, Issue 4. Available online at <https://www.easa.europa.eu/en/downloads/139073/en>. 2022.
- [63] M. Schlosser, H. Braßel, and H. Fricke. “Analysis of Aircraft Ground Trajectories: Map-Matching with Open Source Data for Modeling Safety-Driven Applications”. In: *11th International Conference on Research in Air Transportation (ICRAT)*. Singapore, 2024.
- [64] OpenStreetMap contributors. <https://www.openstreetmap.org>. 2024.
- [65] Edsger W. Dijkstra. “A note on two problems in connexion with graphs”. In: *Numerische Mathematik* 1 (1959), pp. 269–271. url: <https://api.semanticscholar.org/CorpusID:123284777>.
- [66] Peter Hart, Nils Nilsson, and Bertram Raphael. “A Formal Basis for the Heuristic Determination of Minimum Cost Paths”. In: *IEEE Trans. Syst. Sci. Cybern.* 4.2 (1968), pp. 100–107. doi: 10.1109/TSSC.1968.300136.
- [67] Ronald W. Schafer. “What Is a Savitzky-Golay Filter? [Lecture Notes]”. In: *IEEE Signal Processing Magazine* 28.4 (2011), pp. 111–117. doi: 10.1109/MSP.2011.941097.
- [68] Mona Mahboob Kanafi. *Surface generator: artificial randomly rough surfaces*. MATLAB Central File Exchange. <https://www.mathworks.com/matlabcentral/fileexchange/60817-surface-generator-artificial-randomly-rough-surfaces> [Accessed: May 2024].
- [69] Federal Aviation Administration (FAA). *Advisory Circular 150/5380-7B: Airport Pavement Management Program (PMP)*. 2014.
- [70] Federal Aviation Administration (FAA). *Advisory Circular 150/5320-17A: Airfield Pavement Surface Evaluation and Rating Manuals*. Appendix A and B. 2014.

- [71] US Army Corps of Engineers (USACE). *Asphalt and Concrete Surfaced Airfields: Paver Distress Identification Manual*. 2009.
- [72] Transport Canada (TC). *Engineering Reference Document 121: Guidelines Respecting Airport Pavement Structural Condition Survey*. International Aviation & Technical Programs Branch (AARJ). 2004.
- [73] DFS Deutsche Flugsicherung GmbH. *AIP Germany, AD 2: EDDF Frankfurt Main*. AMDT 03/24. 2024.
- [74] DFS Deutsche Flugsicherung GmbH. *Digital Data Sets, Aeronautical Data Germany, AIXM 5.1*. Available online at <https://aip.dfs.de/datasets/>. 2025.